Int J CARS (2013) 8:677–690
DOI 10.1007/s11548-012-0809-z

ORIGINAL ARTICLE

A pilot study on magnetic navigation for transcatheter aortic valve implantation using dynamic aortic model and US image guidance

Zhe Luo · Junfeng Cai · Lixu Gu

Received: 29 October 2012 / Accepted: 20 December 2012 / Published online: 11 January 2013

Abstract
Purpose In this paper, we propose a pilot study for transcatheter aortic valve implantation guided by an augmented magnetic tracking system (MTS) with a dynamic aortic model and intra-operative ultrasound (US) images.
Methods The dynamic 3D aortic model is constructed from the preoperative 4D computed tomography, which is animated according to the real-time electrocardiograph (ECG) input of patient. Before the procedure, the US probe calibration is performed to map the US image coordinate to the tracked device coordinate. A temporal alignment is performed to synchronize the ECG signals, the intra-operative US image and the tracking information. Thereafter, with the assistance of synchronized ECG signals, the spatial registration is performed by using a feature-based registration. Then the augmented MTS guides the surgeon to confidently position and deploy the transcatheter aortic valve prosthesis to the target.
Results The approach was validated by US probe calibration evaluation and animal study. The US calibration accuracy achieved 1.37±0.43 mm, whereas in the animal study on three porcine subjects, fiducial, target, deployment distance and tilting errors reached 3.16 ± 0.55 mm, 3.80 ± 1.83 mm, 3.13 ± 1.12 mm and 5.87 ± 2.35°, respectively.
Conclusion Our pilot study has revealed that the proposed approach is feasible and accurate for delivery and deployment of transcatheter aortic valve prosthesis.

Z. Luo · L. Gu (✉)
School of Biomedical Engineering,
Shanghai Jiao Tong University, Shanghai, China
e-mail: gulixu@sjtu.edu.cn

J. Cai
Department of Cardiosurgery, Ruijin Hospital, Shanghai, China

Keywords Magnetic navigation · Transcatheter aortic valve implantation · Intra-operative US image · Dynamic aortic model · Preoperative planning and registration

Introduction

Aortic stenosis (AS) is the common disorder affecting nearly 5 % of the population aged 75 and above [1]. Its pathology includes processes similar to those in atherosclerosis, including lipid accumulation, inflammation and calcification [2]. AS could result in a high rate of death: Among the untreated patients, approximately 50 % die in the first 2 years after symptoms appear [3]. Surgical replacement of the aortic valve is required to treat symptoms and improve survival in AS patients [4]. Nevertheless, many patients with symptomatic severe AS do not undergo surgery valve replacement due to advanced age or significant comorbidities [5]. Transcatheter aortic valve implantation (TAVI) is a new procedure and less invasive alternative to open heart surgery in which a bioprosthetic valve is inserted into a catheter and delivered through the femoral artery (transfemoral) or the left ventricular apex (transapical) to the diseased native aortic valve to displace and replace the native valve functionally. TAVI offers patients a less invasive alternative enabling valve replacement to be performed without the need for sternotomy or cardiopulmonary bypass [6].

Since 2002, when Cribier et al. [7] first performed the procedure, there has been a progressive trend to use TAVI throughout the world for the treatment of severe AS in patients with high surgical risk. In early 2010, more than 15,000 procedures had been performed globally, mostly confined to these high surgical risk patients [8]. Position of valve during the deployment is paramount to the procedural success, as the optimal positioning of the transcatheter aortic

prosthesis is defined as the displacement and deployment of the native valve leaflets within the native valve annulus [8]. However, the major complications of TAVI are related to poor positioning of the valve during the deployment, including stent malpositioning and migration, coronary obstruction, paravalvular leak, atrioventricular block and aortic root rupture [9]. Optimal positioning of transcatheter valve relies primarily on the anatomical structures of aorta and valve stent intra-operative visualized intuitively. Fluoroscopy (contrast-enhanced fluoroscopy) is commonly used to visualize the aortic anatomy and valve stent to guide the procedure [10]. Fluoroscopy only provides 2D gross images of the aortic valve without 3D context, giving rise to navigational limitations [11], and exposes the clinicians, staff and patient to ionizing radiation. Moreover, contrast agent increases the risk of iatrogenic renal injury [12].

In recent years, several researchers have focused on providing alternative better image guidance for TAVI using intra-operative CT or MRI. Kempfert et al. [13] used C-arm CT augmented fluoroscopy to improve the deployment precision and guide TAVI in 50 patients successfully. However, it still exposed the surgeon and patients to the radiation. Horvath et al. [14,15] had utilized real-time MRI to obtain excellent visualization of anatomical features and achieved TAVI on swine. Although the system provides excellent anatomical visualization, its high cost limits its use in clinical settings.

This study proposes the registration of intra-operative US and a dynamic aortic model in MTS as an alternative approach of guiding TAVI intra-operatively. MTS can provide spatial information on the pose of instruments and US transducers in image-guidance application. It relates these devices to the patient coordinate system so that preoperative plans and images can be registered to, and combined with, real-time imaging modalities [16] and thus enables cardiac intervention using MTS rather than X-ray guidance. Manstad-Hulaas et al. [17] employed navigation technology to deploy stent grafts for treatment of side-branched abdominal aortic aneurysms in phantoms. Abi-Jaoudeh et al. [18] performed thoracic stent-graft deployment for three swine using MTS navigation alone and presented an analysis of accuracy and feasibility. However, the MTS alone cannot recover movement of aorta root during the surgery that could be used to update the preoperative cardiac model.

On the other hand, US imaging is associated with safety, comparatively low cost, ease of use, minimal disruption of the procedure, and lack of compatibility problems between US imaging and standard operating room equipment [19]. Real-time US imaging can provide information relating to the surgical target region in real time. Huber et al. [20] reported simultaneous use of intracardiac and intravascular US to navigate an off-pump aortic valve stent implantation. However, the limitation of resolution and field of view makes the US images hard to interpret. To improve the interpretability of US images, Lang et al. [21] constructed an augmented image guidance for TAVI by registering together TEE US image and a static cardiac model derived from preoperative CT. Confined to the movement of aortic valve, the final precision of aortic valve prosthesis placement could be compromised.

Here, we combine the MTS with the dynamic aortic model and the real-time US image for guidance of position and deployment of transcatheter aortic valve prosthesis intra-operatively. Instead of using traditional fluoroscopy guidance, the deployment is guided by a multimodality MTS that integrates 2D US images with corresponding 3D context by registering them to preoperative dynamic aortic model derived from the preoperative 4D CT image. After a dynamic 3D aortic model has been constructed, spatial and temporal registrations are performed to map the patient coordinate to the model coordinate. The dynamic model is animated corresponding to the real-time input of ECG signals. Prior to the introduction of intra-operative US images, the US probe calibration is performed to calculate the transformation that maps the US image coordinate to the tracked device coordinate. The temporal alignment is performed to synchronize the ECG signals, intra-operative US image and tracking information, so that the spatial registration could be performed by a feature-based registration assisted by the synchronized ECG signals. Finally, the augmented MTS guides the surgeon to confidently position and deploy the prosthesis to the target. We believe that this is the first application on TAVI using US imaging assisted by the augmented MTS.

Methods

Calibration of US probe

Prior to the introduction of the US images, the US probe must be calibrated to confirm the transformation from the US image coordinate to that of MTS tracking sensor attached to the US probe. The transformation can be defined as:

$$\begin{pmatrix} x_{\mathrm{w}} \\ y_{\mathrm{w}} \\ z_{\mathrm{w}} \\ 1 \end{pmatrix} = \mathrm{TM}_{\mathrm{world}\leftarrow\mathrm{td}} \cdot \mathrm{TM}_{\mathrm{td}\leftarrow\mathrm{ui}} \begin{pmatrix} s_x \cdot u_k \\ s_y \cdot u_v \\ 0 \\ 1 \end{pmatrix} \quad (1)$$

where $\mathrm{TM}_{\mathrm{td}\leftarrow\mathrm{ui}}$ is the transform matrix from the US image coordinate to that of the tracking device which is a standard 6DOF sensor attached on the US probe as shown in Fig. 1a, and the $\mathrm{TM}_{\mathrm{world}\leftarrow\mathrm{td}}$ is the transform relating the tracking device to the world coordinates defined by the MTS. (u_k, u_v) represents a point in the US image, and s_x, s_y are the scale factors of the x and y axes, respectively. This point can be transformed to its corresponding point $(x_{\mathrm{w}}, y_{\mathrm{w}}, z_{\mathrm{w}})$ in the world coordinate by Eq. 1. $\mathrm{TM}_{\mathrm{world}\leftarrow\mathrm{td}}$ is updated according to the probe pose and acquired from MTS in real time.

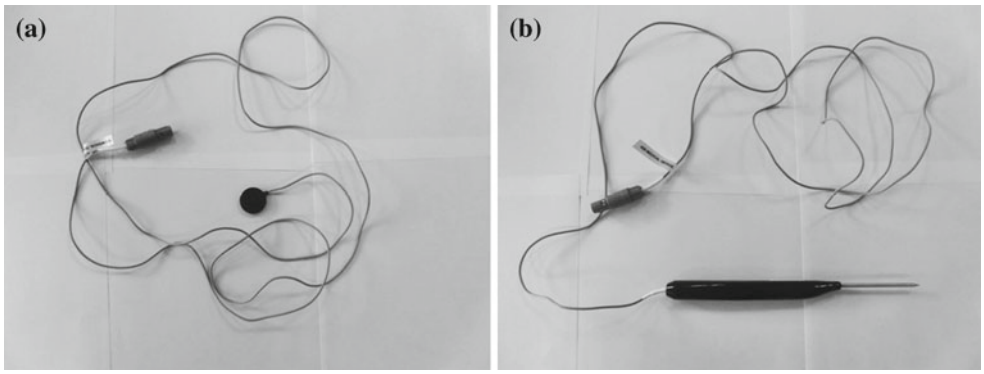

Fig. 1 The tracked instruments used for US calibration. **a** The 6DOF sensor. **b** The 6DOF pointer

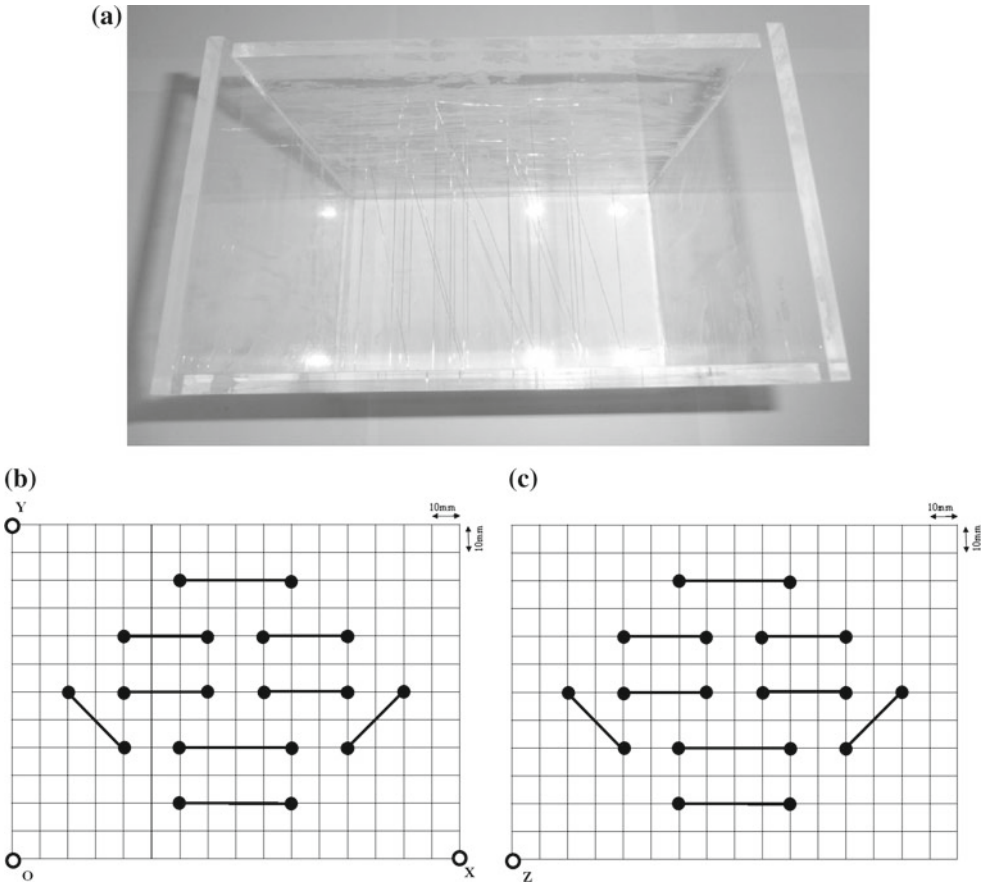

Fig. 2 The calibration phantom. **a** The calibration phantom. **b** and **c** The front and back inner walls of the phantom in a grid form. Each grid is 10 mm × 10 mm. The *black disk* (so called end point) is the hole to fix the end of copper wire. Each couple of disks connected by a *solid line* constructs a *N shape* structure. After obtained the positions of O, X, Y and Z in MTS coordinate using the pointer, the positions of the end points in MTS coordinate can be calculated according to their position in the orthogonal coordinate OXYZ

$TM_{td \leftarrow ui}$ is a constant once the 6DOF sensor is attached on the probe. A calibration operation is required to measure the $TM_{td \leftarrow ui}$.

Our previous work [22] has implemented a calibration system using the 2D alignment method [23,24] to calibrate the probe, the operation of which is tedious and time consuming. Here, we designed an improved calibration phantom using a freehand method [25] which is simpler, faster and more accurate.

As shown in Fig. 2a, the calibration phantom contains several 0.2-mm-diameter copper wires, which are stretched between holes of diameter 0.6 mm in the front and back walls of the phantom with a same layout as shown in Fig. 2b, c. These wires construct eight N-shaped structures made up of

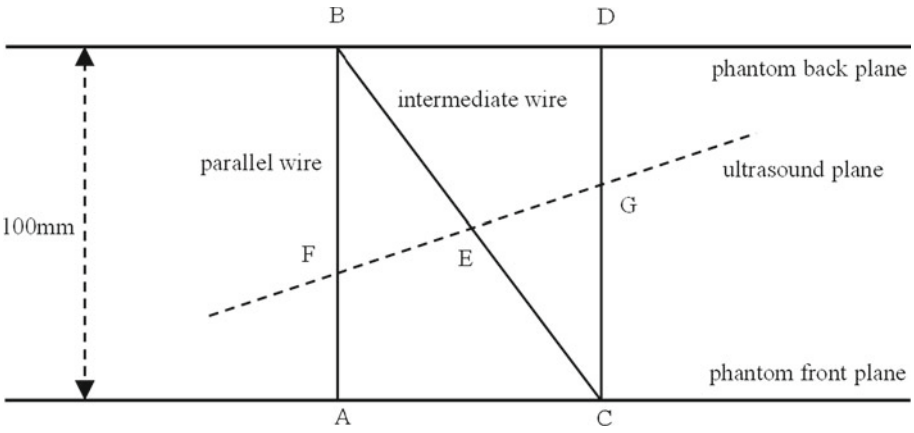

Fig. 3 The intersection between a *N shape* structure and US plane

two parallel wires and one intermediate wire. In order to get the position of each end point inside the phantom wall in MTS coordinate, four pits O, X, Y and Z with the diameter of 0.3 mm are marked in the inner side of the front and back walls. During the calibration, a MTS-tracked pointer (Fig. 1b) is used to get the positions of the pits to determine an orthogonal coordinate. O is the origin. $\vec{OX}$, $\vec{OY}$ and $\vec{OZ}$ are the orthogonal axes. Therefore, each position of end points in MTS coordinate can be calculated in this orthogonal coordinate.

As shown in Fig. 3, the E, F and G, which are the intersection points between the wires BC, AB, CD and the US plane, are unknown. However, E can be determined in the phantom coordinate system by the following set of Eq. 2:

$$\begin{cases} x_E = x_B + k \times (x_C - x_B) \\ y_E = y_B + k \times (y_C - y_B) \\ z_E = z_B + k \times (z_C - z_B) \end{cases} \quad (2)$$

where k is the length ratio of BE–BC. Because wires AB and CD are parallel, the triangles BEF and CEG are similar, so that

$$k = \frac{|BE|}{|BC|} = \frac{|FE|}{|FG|} \quad (3)$$

Points E, F and G can be defined in the US image, and the lengths of FE and FG can be calculated to get the positions of E (defined as key point) in both US and MTS coordinate.

The calibration phantom has eight N-shaped structures. When we fixed the US probe, the US plane intersected with these structures (Fig. 4). For each key point P_j, we got its position p_{ui}^j in US image coordinate and p_w^j in MTS coordinate, $j = 1, \ldots, 8$. They were used to calculate the probe calibration matrix $TM_{td \leftarrow ui}$ in Eq. 4:

$$TM_{td \leftarrow ui} = \arg\min_{TM} \sum_{j=1}^{N} |TM_{world \leftarrow td} \cdot TM \cdot p_{ui}^j - p_w^j|^2 \quad (4)$$

using a direct least squares error minimization technique [26].

Fig. 4 The scenario of US probe calibration

Dynamic aortic model

The dynamic aortic model was constructed based on the 4D CT image of the beating heart over a cardiac cycle with retrospective ECG gating. Ten 3D CT images covering a beating heart cycle, which are high resolution and enhanced by contrast agent injections, were acquired using a TOSHIBA Aquiline ONE CT with imaging parameters: slice thickness = 0.5 mm, pitch = 0.237, kVp of view = 22 cm, image resolution = 512 × 512 and spacing = 0.653 mm × 0.653 mm × 0.25 mm. To minimize the heart motion artifacts, the end-diastolic (ED) image of the 4D dataset was chosen to create a static model, where a manual segmentation was performed slice-by-slice using a "paint pen" technique to outline the aortic structure. Then a non-rigid registration [27] using trilinear interpolation and downhill simplex optimizer was performed to register the ED image to each of the remaining images along the 4D dataset. Finally, the registration transformations were used to deform the static initial model to

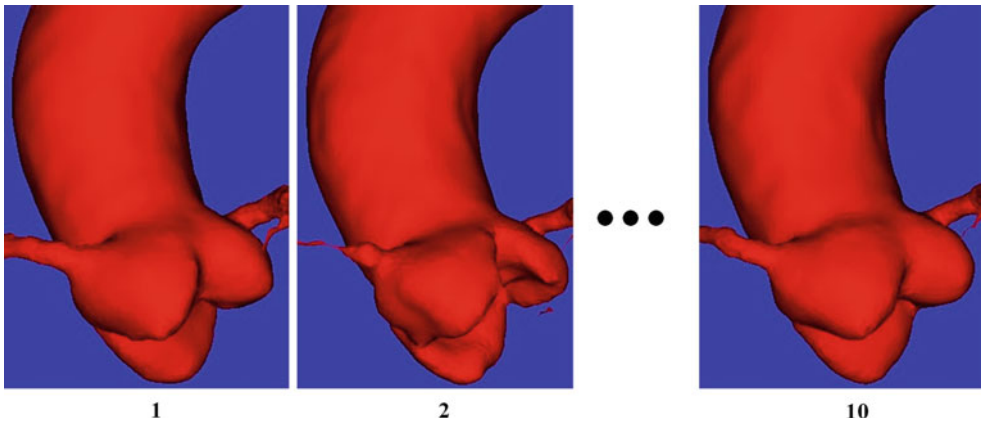

Fig. 5 A dynamic aortic model of a cardiac cycle

build the dynamic aortic model which consisted of 10 static models (Fig. 5).

Temporal synchronization

Due to different sampling delay in the US images, ECG signals and tracking information acquisition, the readings from different inputs may not be corresponding to the same cardiac phase even at the same time point. A temporal alignment [19] was performed to calibrate and compensate the temporal latency between the US images, ECG signals and tracking information. In that way, the cardiac phase of each input US image can be analyzed, and its corresponding aortic model can be matched using a nearest-neighborhood interpolation.

Preoperative planning

Prior to the surgery, the surgeon performed the preoperative planning on the preoperative images to determine the optimal position of the prosthesis. The structure of the prosthesis is shown in Fig. 6, which has three nadir leaflets. A pericardial skirt covering the lower segment of the prosthesis from the inflow to the nadir of the leaflets is designed to prevent paravalvular regurgitation.

For each preoperative CT image, the three nadirs of the leaflets were identified manually (Fig. 7a) and used to determine the annular plane (Fig. 7b). Then the annular plane was translated along its normal toward left ventricle (LV). The translation distance was half of the height of the skirt (6 mm), and the final plane was defined as the target position (Fig. 7b) in the dynamic aortic model.

Aortic root contour extraction

The aortic valve contour in the intra-operative US image was required to be segmented, so that the US image could be registered to the preoperative dynamic aortic model using the feature-based registration intra-operatively.

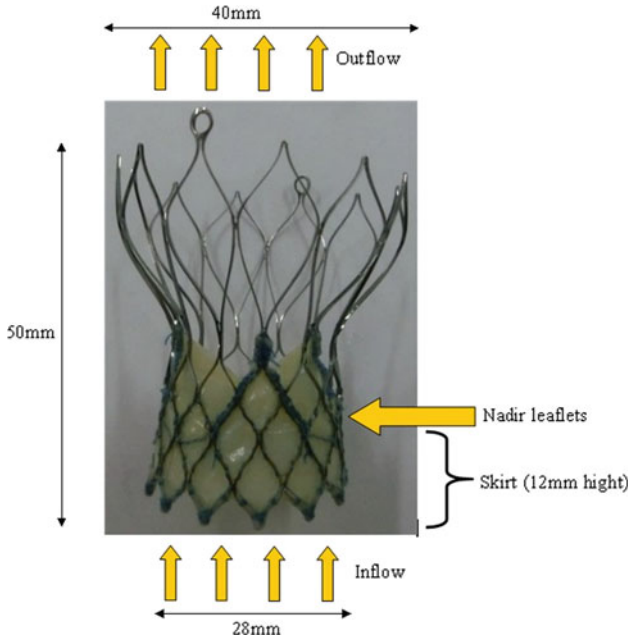

Fig. 6 The transcatheter aortic valve prosthesis. A pericardial skirt, which is designed to prevent paravalvular regurgitation, covers the lower segment of the aortic valve prosthesis from the inflow to the nadir of the leaflets

A graphic processing unit (GPU) accelerated continuous max-flow algorithm [21,28] was employed to automatically segment the aortic root from intra-operative US image of the long view and short view in approximately real time (less than 40 and 120 ms for 320×240 and 640×480 US image, respectively) as shown in Fig. 8. Comparing to the classic max-flow algorithm, it avoids grid bias, increases the segmentation accuracy and can be implemented in a parallel manner by graphic card [29].

Spatial registration

Registration between the 2D intra-operative US image and the preoperative dynamic aortic model was performed to

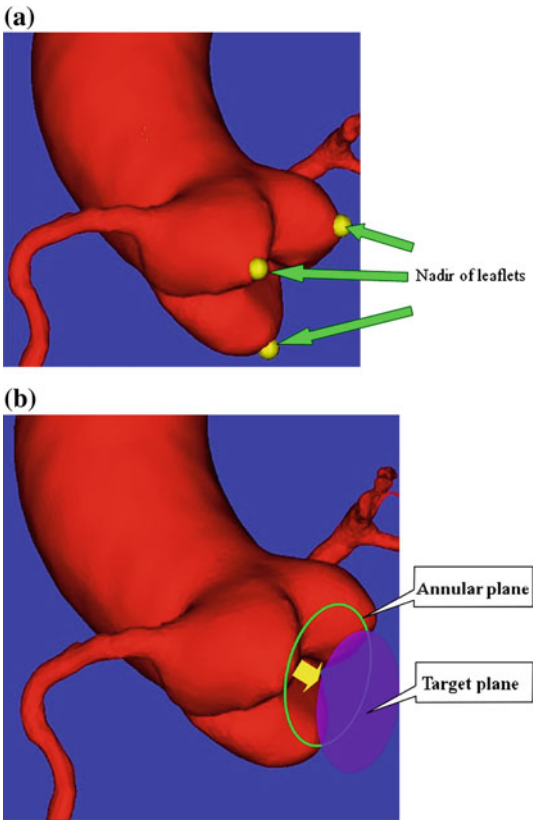

Fig. 7 The preoperative planning. **a** Find the three nadirs of leaflets (the *yellow points*). **b** Define an annular plane (*green circle*) by the *three yellow points*, and then translate the plane toward LV 6 mm to get the final target plane (*pink disk*).

compensate the error derived from the respiration and the movement of aortic root.

Most intensity-based registration algorithm is always formulated as an optimal problem where a global optimal transformation between two images is calculated using a specific similarity metric such as the mutual information (MI). However, major complaints lie in the problem of local minima and slow convergence rate. The low quality of US image could further complicate and prolong the registration process. Hence, we used the feature (contour) extracted from intraoperative US image to conduct the registration.

The registration consists of two steps, initial and intra-registration. The initial registration provides the intra-registration a fine start point to converge quickly without stuck into the local minima as shown in Fig. 9a, b.

1. Initial registration
   A fiducial landmark registration was performed to minimize the mean-squared distance between homologous landmarks in the preoperative image and patient's (world) to get an initial transformation $TM_{image \leftarrow world}$. For the same reason described in section "Dynamic aortic model," ED image of the preoperative 4D dataset was chosen in this operation. Based on the temporal alignment between the US images and ECG signal acquisition, a series of US images of aortic root at short- and long-axis view with their cardiac phases were acquired. Each of the US images was associated with a preoperative aortic model according to its cardiac phase. In order to get a better initial transform, every aortic model was associated with at least one US image of long-axis view and one of short-axis view. Then the contour of aortic root in each US image was manually selected. The points of all contours were transformed to preoperative image coordinate using $TM_{image \leftarrow world} * TM_{world \leftarrow td} * TM_{td \leftarrow ui}$. Then, these transformed contours were divided into 10 groups with their corresponding cardiac phases related to their aortic surface model. All the synchronized pairs of transformed aortic root contours and surface models were registered using a feature-based registration—Iterative Closet Points (ICP)—and the transformations $TM_i\,(i = 1, \ldots, 10)$ were obtained. Thus, each 3D model within the preoperative dynamic aortic model was associated with a transformation $TM_i'(=TM_i * TM_{image \leftarrow world})$, which mapped the patient coordinate to the preoperative

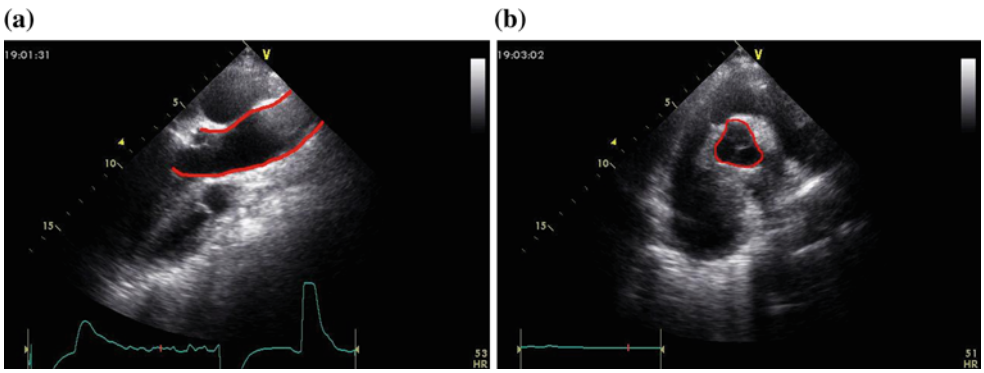

Fig. 8 Extract *aortic root contour* from US image. **a** Extracted *contour* from US image of long-axis view. **b** Extracted *contour* from US image of short-axis view

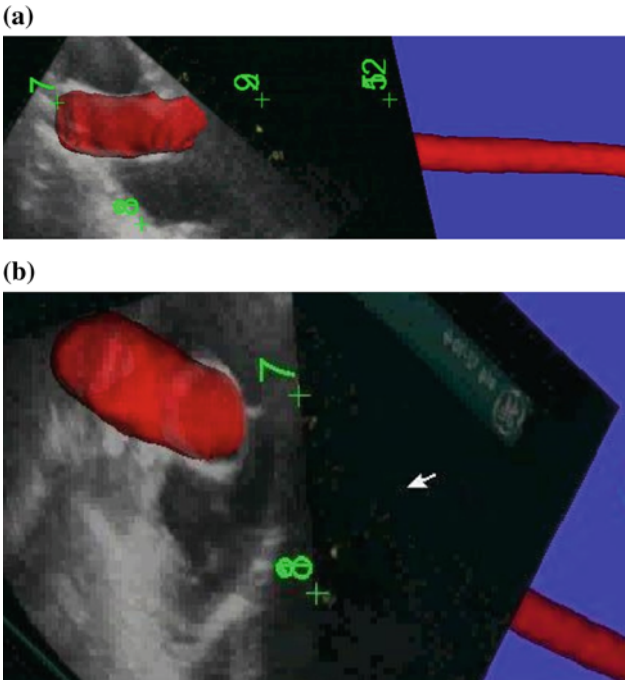

Fig. 9 Registration using intra-US image. **a** Register using long-axis-view US image. **b** Register using short-axis-view US image

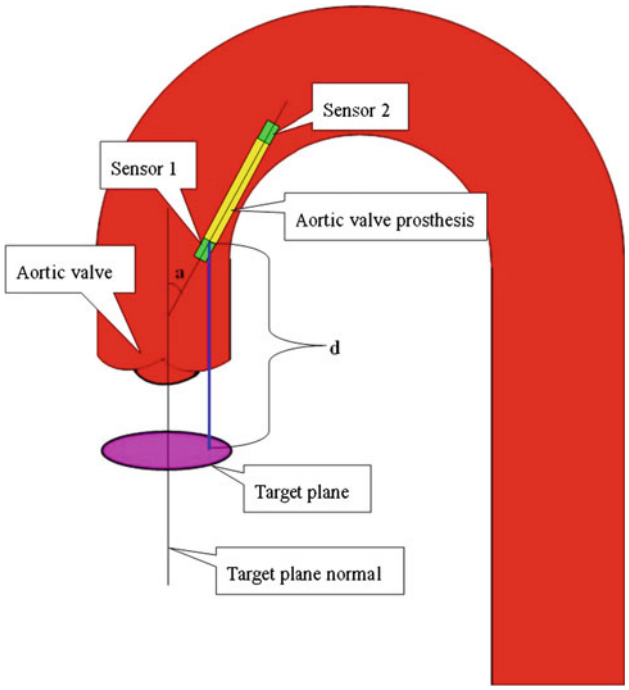

Fig. 10 The layout of the navigation. The *blue line* segment perpendicular to the target plane represents the distance **d** from the *top point* of folded aortic valve prosthesis to the target plane, and *the angle* **a** represents the *angle* between the normal of target plane and the direction of aortic valve prosthesis

image coordinate as an initial transformation for intra-registration.

2. Intra-registration
   The objective of intra-registration is to register the intra-operative US image to preoperative dynamic aortic model rapidly. During the procedure, each real-time US image of long- or short-axis view, from which the aortic contour was extracted automatically, was acquired and associated with its corresponding cardiac phase i. The points of the contour were transformed by $\mathrm{TM}_i' * \mathrm{TM}_{\mathrm{world}\leftarrow\mathrm{td}} * \mathrm{TM}_{\mathrm{td}\leftarrow\mathrm{ui}}$. Then the transformed points were registered to the surface model at phase i using the ICP algorithm to get a new transformation TM_i''. The transformation from patient (world) coordinate to the preoperative 4D CT image (dynamic aortic model) coordinate was updated frequently via $\mathrm{TM}_i'' * \mathrm{TM}_i'$ during the navigation. This whole process was implemented in a parallel manner.

Navigation

Following preoperative planning, US probe calibration, temporal and spatial registration, the prosthesis and target plane were displayed in an augmented reality (AR) environment of the navigation system as shown in Fig. 10, where the target plane is depicted in pink, the blue line segment perpendicular to the target plane represents the distance from the top point of folded aortic valve prosthesis to the target plane, and the angle a represents the angle between the normal of target plane and the direction of aortic valve prosthesis. The navigation system monitored and reported the distance and the angle. During the surgery, the 5DOF sensors provided an intuitive depiction of the orientation and position of the prosthesis in the aorta.

Component

1. Transcatheter aortic valve prosthesis
   The transcatheter aortic valve prosthesis (MicroPort., Shanghai, China) we used is a self-expanding valve stent frame, which is composed of nitinol with porcine pericardial leaflets as demonstrated in Fig. 6. It expands at normal temperature, but can be compressed in ice water to fit inside a catheter.
2. Catheter
   The catheter (MicroPort., Shanghai, China) we used is 18F. As shown in Fig. 11, two 5DOF sensors are embedded in the front part of the catheter. The prosthesis is compressed and embedded into the catheter between the two 5DOF sensors so that the MTS can track the position and orientation of prosthesis when the catheter is inserted into the aorta.
3. Tracking device
   An Aurora MTS (North Digital., Waterloo, On, Canada) is employed to track the position and orientation of both the catheter and the US probe. A standard 6DOF (Fig. 1a)

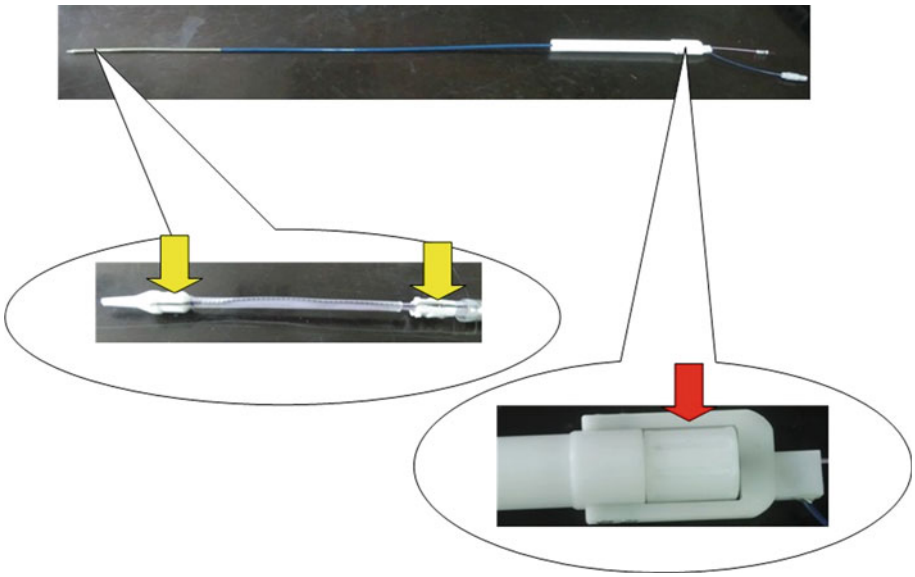

Fig. 11 The catheter used in this study. The *two yellow arrows* indicate the location of the 5DOF sensors. The *red arrow* indicates the knob to release the aortic valve prosthesis

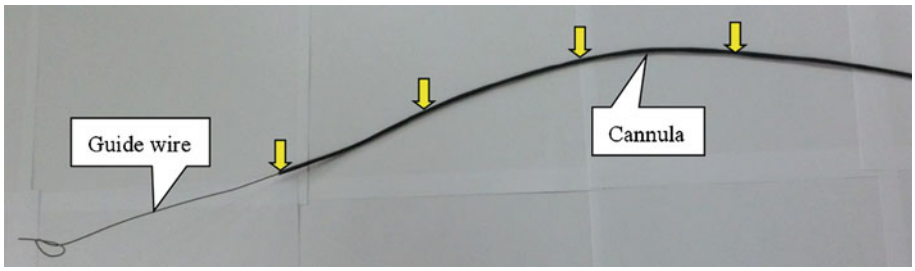

Fig. 12 The guided wire and cannula. The *four yellow arrows* indicate the location of sensors in the cannula

sensor is mounted onto the US probe for US image tracking.

4. Guide wire and cannula
   Prior to the insertion of the catheter in which prosthesis is included, a guide wire is advanced from the common femoral artery access into the aortic root. The guide wire is enclosed by a cannula in front of which four MTS 5DOF sensors are embedded to enable tracking (Fig. 12). The positions of these four 5DOF sensors are used to fit a cardinal spline to create a model of the front part of the cannula that can be displayed in the AR environment, which makes the surgeon aware whether the cannula passed through the aortic arch or not. When the cannula arrives at the aortic root, it is extracted, while the guide wire remains. Then the catheter is inserted into the aorta along the guide wire until it arrives at the aortic root.
5. ECG reading device
   A handled ECG reader device (Beijing Choice Electronic Tech, Beijing, China) (Fig. 13) was used to sample cardiac phases of subject intra-operatively.
6. Software
   The software for this system is based on our previously developed navigation system [30] using Python 2.7, and

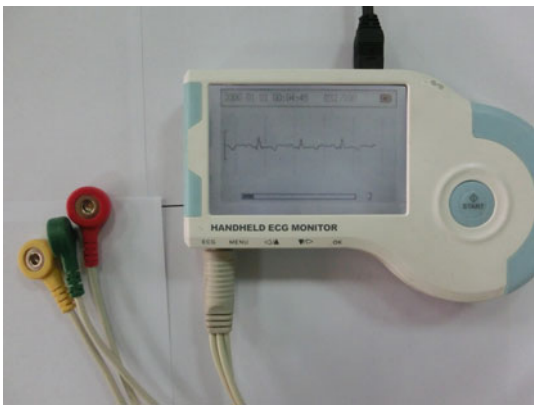

Fig. 13 The ECG reader

third-party libraries from the Visualization Toolkit: VTK 5.6 (http://www.vtk.org), Atamai (http://www.atamai.com) and Compute Unified Device Architecture (CUDA 4.0). The system runs under Windows XP, on an Intel Core i5 computer with NVIDIA GeForce GTX 560 graphics card with 1 GB display memory and 256 bit width. Intra-operative US images were acquired using a GE Vivid 7 US machine, with the images being integrated into our navigation system after probe calibration.

The system displays the 4D aortic surface model of patient, along with a semitransparent calibrated US image plane to construct an AR environment to provide an updated interior view of the aorta in real time. The model of the prosthesis is also displayed in the system after insertion into the aorta. Its distance from the target position is also monitored and shown.

Results

Evaluation of US probe calibration

To evaluate the probe calibration, we measured a 3D navigation accuracy (3D NAC) [25] to determine the quality of the proposed calibration. The 3D NAC compares points, which are transformed from US image coordinate to world coordinate, to the physically measured coordinates directly and is defined as:

$$\Delta_{\text{3D NAC}} = \underset{j}{\text{mean}}\{||\text{TM}_{\text{w}\leftarrow\text{td}} \cdot \text{TM}_{\text{td}\leftarrow\text{ui}} \cdot p_{\text{ui}}^{j} - p_{\text{w}}^{j}||\} \tag{5}$$

where $\Delta_{\text{3D NAC}}$ is the 3D NAC, $\text{TM}_{\text{w}\leftarrow\text{td}}$ is the transformation from the tracked device (the 6DOF sensor) coordinate to world coordinate, $\text{TM}_{\text{td}\leftarrow\text{ui}}$ is the transformation from the US image coordinate to the tracked device coordinate, while p_{ui}^{j} and $p_{\text{w}}^{j}(j = 1, 2, \ldots, \text{N})$ are the positions of the points in the US and world coordinate, respectively.

A calibration panel was used to compute the 3D NAC. The panel contains 25 polyvinylchloride (PVC) cylinders of 1.5 mm radius and 1 mm height (Fig. 14a). Each cylinder contains a 0.5-mm divot within its exposed surface and is inserted into the panel in 1-mm-deep holes. After the probe calibration was performed, the 3D NAC was measured by placing it in several positions with different orientations. In each position, the US plane was aligned to the plane defined by the centers of cylinders in the panel as shown in Fig. 14b. The alignment between the two planes was defined that all the cylinders can be seen in the US plane. Then the position p_{ui}^{j} of each cylinder center was identified manually in the US image, and the position p_{w}^{j} in world space was detected by the tracked pointer. Afterward, all the p_{w}^{j} and p_{ui}^{j} were used as inputs to Eq. 6 to calculate the 3D NAC.

Table 1 shows the results of 3D NAC, demonstrating an average accuracy of 1.37 ± 0.43 mm.

Animal study

Further validation was achieved by a porcine study which performed prosthesis deployment on three swine and measured four errors. Our animal experiment was authorized by the committee of ethic in Shanghai municipal and Shanghai Jiaotong University with certification number of SYXK (HU) 2007-0025.

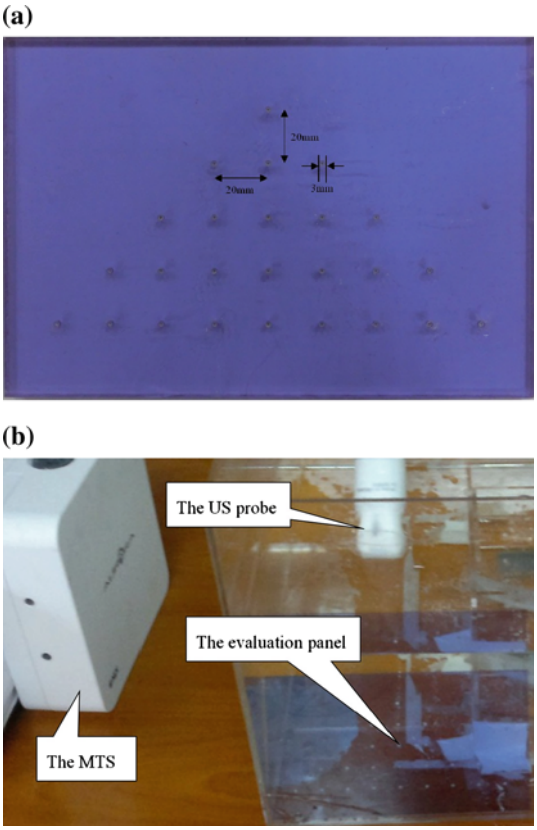

Fig. 14 Evaluation of US probe calibration. **a** The evaluation panel. **b** One position of the panel to evaluate the error

1. Fiducial registration error (FRE)
   FRE was assessed in each case by calculating the root mean square (RMS) of the difference between the fiducial marker positions in image space and their registered positions in world coordinate [26]. FRE is defined in Eq. 6:

$$\text{FRE} = \frac{1}{N}\sum_{i=1}^{N} |T x_i - y_i| \tag{6}$$

   where N is the number of source points and T is the transform between the world coordinate and the preoperative CT image coordinate. The fiducial registration algorithm finds the transform T that minimizes the FRE. The FRE will be reported from the navigation system automatically after registration.
2. Target registration error (TRE)
   TRE defines the misregistration error between the tracked device location reported by the system and its actual location. The TRE was measured by advancing the tracked cannula from the common femoral artery access to the

Table 1 The result of 3D NAC

Position	Point 1	Point 2	Point 3	Point 4	Point 5	Point 6	Point 7	Point 8	Point 9	Point 10
1	1.35	1.52	1.72	2.12	1.28	1.11	0.94	1.87	0.98	0.77
2	0.95	2.01	1.84	0.88	0.56	1.88	1.57	0.87	1.23	0.98
3	1.81	0.82	2.15	1.55	1.84	1.36	0.84	1.57	1.79	1.23
4	1.12	0.91	1.85	1.95	1.39	1.30	0.96	0.79	1.71	1.36
5	1.63	1.13	1.26	1.69	1.22	0.76	1.27	0.93	2.05	1.91

aortic root after registering the pig's preoperative 4D CT image to world coordinate using registration method described above. The locations $p_{\text{navi}}^{i,j}$ ($i = 1, 2, 3, 4$; $j = 1,2,\ldots,N$, where N is the number of phases in a cardiac cycle) of the four 5DOF sensors in each phase of a cardiac cycle were reported by the system. We then fixed the cannula inside the aorta, and the postoperative 4D CT image was scanned. For each pair of preoperative and postoperative 3D CT images, we performed a rigid registration using the fiducial landmarks in these images to get an initial transformation. Based on the transformation, a MI registration using trilinear interpolation and powell optimizer, of which transformation was affine, was employed to refine the registration from the postoperative image to the preoperative image to achieve the final transformation TM_j. Because the 5DOF sensors can be easily identified in the CT image, their positions $p_{\text{post}}^{i,j}$ in the postoperative image coordinate system were measured and considered as the ground truth. For each cardiac phase j, we transformed the $p_{\text{post}}^{i,j}$ by $p_{\text{pre}}^{i,j} = \text{TM}_j \cdot p_{\text{post}}^{i,j}$, where $p_{\text{pre}}^{i,j}$ are their positions in the preoperative image coordinate. The TRE of each cardiac phase was then computed by:

$$\text{TRE}_j = \frac{1}{M}\sum_{i=1}^{M} |p_{\text{pre}}^{i,j} - p_{\text{navi}}^{i,j}| \tag{7}$$

where M is the number of 5DOF sensors in the cannula.

3. Deployment distance error (DDE)
   DDE is defined as the difference between actual final prosthesis position and preoperative planning deployment position. DDE was measured as the distance from the leading edge of transcatheter aortic valve prosthesis to the target plane in the postoperative CT coordinate system.
4. Deployment tilting error (DTE)
   DTE is defined to evaluate how well the system can help to position the valve in the aortic root anatomy with a correct tilting. DTE was measured as the angle between the normal of target plane and normal of the plane defined by the leading edge of the prosthesis in the postoperative CT coordinate system.

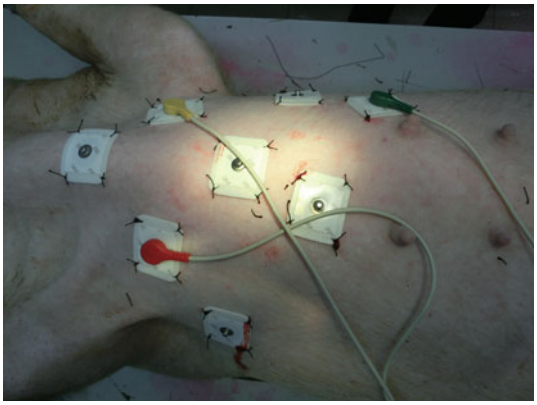

Fig. 15 The fiducial landmarks

In each case, the four measurements were employed to calculate the final errors.

The details of the experiment are as follows.

Pigs weighing between 70 and 80 kg were selected for the experiments. Eight fiducial landmarks, which are ECG electrodes, were attached on the skin in the area of the rib cage (Fig. 15). The animals were anesthetized, and the heart rate was reduced to 90–100 beats/min by injected Betaloc (5 mg:5 ml, Vetter Pharma-Fertigung Gmbh & CoKG, Germany) during the procedure. Respiration was controlled by a mechanical ventilator at 15–20 cycles/min.

The preoperative dynamic aortic model of the animal was reconstructed using the method described earlier and then imported into the navigation system. Preoperative planning was performed on the model, and the target position of prosthesis was determined.

Finally, the calibration of the US probe was achieved using the calibration phantom to fuse the real-time US image with the CT image, and the registration described above was performed. Then the tracked guide wire was advanced from the common femoral artery access to the aortic root. When the cannula arrived at the aortic root along with the guide wire, the former one was removed. Afterward, the catheter entered the aorta along the guide wire. Under the guidance of the system and the fused real-time US image (Fig. 16), the surgeon was able to confidently reach the target position and release the transcatheter aortic valve prosthesis to the

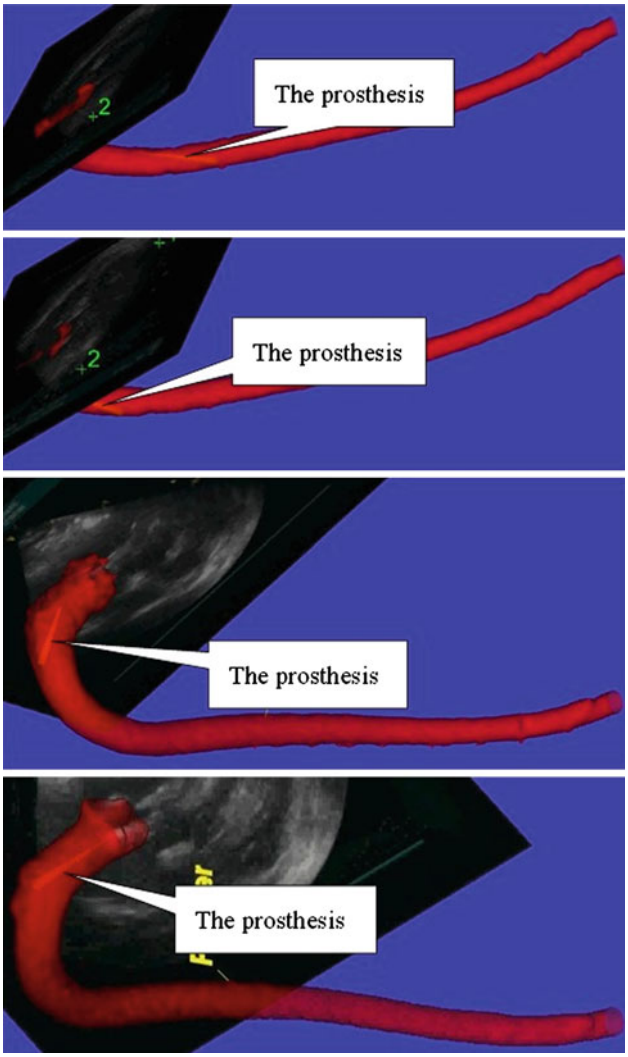

Fig. 16 The guidance of system

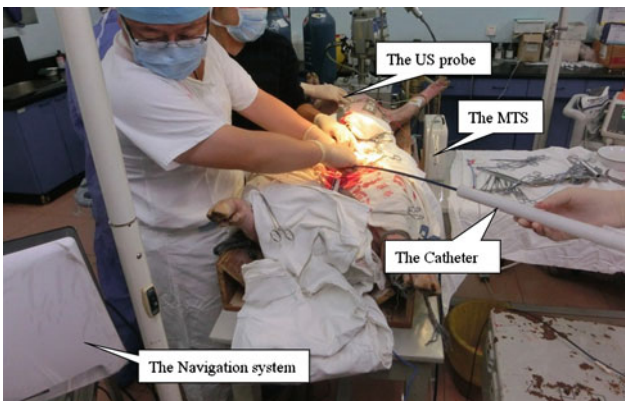

Fig. 17 The scenario of the surgery

correct position (Fig. 17). After the operation, the postoperative CT image (Fig. 18) was examined to determine the DDE and DTE. The FRE is 3.16 ± 0.55 mm (Table 2), the TRE

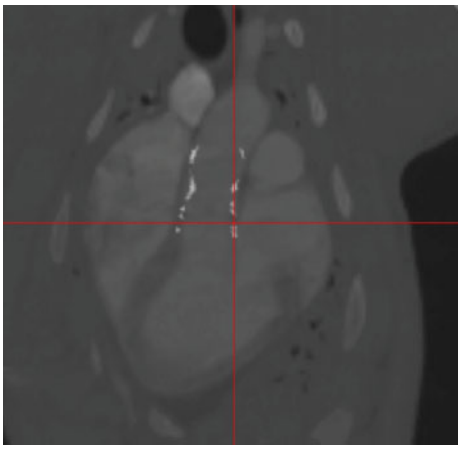

Fig. 18 Postoperative evaluation

Table 2 The result of FRE

	Case 1	Case 2	Case 3
FRE	2.6	3.2	3.7

is 3.80 ± 1.83 mm (Table 3), the DDE is 3.13 ± 1.12 mm (Table 4), and DTE is 5.87 ± 2.35° (Table 4).

Discussion

Evaluation of US probe calibration

During the US probe calibration, the errors mainly came from two sources. First, to localize the positions of the end points of the copper wires in the US probe calibration, the probe calibration used a pointer, whose tip was tracked by MTS to obtain these positions in real-world space, similar to the fiducial landmark registration. And the tip's position was calculated according to its tip position relative to the coordinate of the 6DOF sensor attached in its axis. The relative position of its tip was acquired using a "pivot" operation which was performed manually using a "NDI Tool Tracker" software provided by North Digital (Waterloo, On, Canada), which can report the tip offset and RMS error [31] less than 0.3 mm in this research. Second, another source error originated from identification of intersection between the US plane and the copper wires in US image, which should be less than 0.2 mm because the diameter of the copper wires is 0.2 mm.

Evaluation of animal study

There are other four errors measured in this research: FRE, TRE, DDE and DTE.

The TRE represents the real error of the registration. Specification of selection of points for rigid landmark-based

Table 3 The result of TRE

Case	Phase 1	Phase 2	Phase 3	Phase 4	Phase 5	Phase 6	Phase 7	Phase 8	Phase 9	Phase 10
1	5.31 ± 1.81	6.33 ± 2.04	4.83 ± 1.28	4.68 ± 1.77	3.43 ± 1.28	3.45 ± 1.75	2.63 ± 1.35	2.80 ± 0.88	1.85 ± 0.53	2.33 ± 1.22
2	5.65 ± 1.50	5.60 ± 1.88	5.13 ± 1.49	4.50 ± 1.83	4.13 ± 1.41	4.08 ± 1.01	2.78 ± 1.39	3.05 ± 1.04	2.10 ± 0.94	2.43 ± 1.62
3	5.33 ± 1.66	4.65 ± 2.19	4.75 ± 2.31	4.56 ± 1.85	3.9 ± 51.95	3.3 ± 32.07	2.98 ± 0.96	2.68 ± 1.31	2.2 ± 31.28	2.63 ± 1.15

Table 4 The result of DDE and DTE

	Case 1	Case 2	Case 3
DDE	+1.9	+4.1	+3.4
DTE	3.3	6.4	7.9

registration in image and real space, co-registration between preoperative images and postoperative images, pivot operation and respiration are the main factors influencing the TRE. The registration used in this research is mainly based on ICP registration algorithm whose accuracy and convergence rate depend on the initial transformation. The respiration is a major factor that affects the output of the initial registration. A ventilator was used to reduce its impact in this study.

The overall accuracy of the system was measured by the DDE and DTE, to which the FRE and TRE also contributed, where the DDE of our research was 3.13 ± 1.12 mm. The result in Table 4 shows the prosthesis deviated toward LV in all cases, which was caused by two reasons. First, the human-oriented prosthesis we used was unsuitable for porcine. The diameter of the outflow of aortic valve prosthesis was much bigger than the diameter of swine's aorta root (sinotubular junction and the tubular part of aorta close to it). Consequently, after the release of aortic valve prosthesis, the pressure of the vascular wall made it slide toward LV. Second, the calcification of aortic valve contributed to the fixation of the aortic valve prosthesis in the aorta valve. However, the porcine subjects were healthy without calcification. The DDE we achieved was less than 4mm, which could be considered as a good clinical result. For the DTE, a tilting of less than 5° is regarded as very good, $5° - 10°$ as good, $10° - 15°$ as acceptable and larger than 15° as inappropriate [32]. The DTE of our study was $5.87 \pm 2.35°$, with two cases within $5° - 10°$ and one less than 5°.

Guidance

Besides the traditional deployment via fluoroscopic guidance, there are three possible methods to guide the prosthesis deployment: US guidance only, MTS image guidance only and MTS plus guidance.

For the US guidance only method, the 2D intra-operative US image can provide the real-time information of the surgical target region, allowing the surgeon to judge from the US image whether the position of the prosthesis is at the target position or not. However, three factors make this guidance a failure in most cases. The first one is the air in the lung and intestines, which makes it very difficult to see the descending aorta in the US image. Second, prior to the arrival at the aortic root, the guide wire (catheter) has to pass the aortic arch which is a region uneasily seen in the US image. Third, because of the complexity of the target region and the low quality of the US image, it is also hard to identify the guide wire. Our trials of all three cases using only US guidance failed. In each case, when the guide wire was inserted into the descending aorta, we lost the position of its tip owing to the invisibility of descending aorta in US image. In addition, because of the low quality of the US image in the aortic arch, we could not guarantee the guide wire had passed through the aortic arch, leading to failure in the surgery.

For the MTS guidance only method, since the deformation of descending aorta and aortic arch is slight (the maximum average diameter change of descending aorta between an RR interval is less than 2 mm [33]), we believe the virtual model augmented by the MTS-tracked guide wire can pass through the aortic arch and arrive at the aortic root to guide the catheter. But the aortic root moves intensely within the cardiac cycle. Without intra-operative imaging, the MTS guidance only method is based on a sole rigid transformation, which can hardly compensate the error derived from movement of aortic root intra-operatively. Moreover, the respiration adds the registration error, making it unable to guarantee the deployment accuracy.

The proposed approach combined MTS with real-time US, which provides a flexible platform for registering intra-operative US images with preoperative dynamic aortic model spatially and temporally to compensate the lack of direct vision during deployment of the prosthesis. The MTS system guides the guide wire with cannula to the aortic root. With the cannula extracted, the guide wire guides the MTS-tracked catheter to the aortic root. The quality of US image is relatively better in aortic root, where the contour of aortic root can be identified easily. The synchronized intra-operative US image is introduced and registered to the dynamic aortic model according to the ECG signals. The intra-registration compensates the errors caused by aortic root movement and respiration to guarantee the final deployment accuracy. With the complementary information captured in two different

modalities, the results of our approach are safer, more stable and clinically applicable.

So far, the segmentation is manually performed which could be improved by using a more sophisticated algorithm in the future. More animal studies are scheduled to better investigate the possibility of the clinical application.

Conclusion

This paper proposed an MTS enabled navigation system for transcatheter aortic prosthesis deployment using intra-operative US imaging and dynamic aortic model. The pilot animal study results reveal that this method could be another possible option for delivery and deployment of an aortic prosthesis.

Acknowledgments This research work is partially supported by the Chinese NSFC research fund (61190120, 61190124 and 61271318), the Shanghai municipal health bureau research fund (2011216) and Biomedical engineering fund of Shanghai Jiaotong University (YG201 2MS21). The authors are grateful to the radiologists from Zhongshan Hospital for their support in animal imaging and animal surgery as well as to MicroPort Co., Ltd. for providing and renewing cannula, transcatheter and aortic valve prosthesis for MTS guidance purpose.

Conflict of interest None.

References

1. Nkomo VR, Gardin JM, Skelton TN et al (2006) Burden of valvular heart diseases. Lancet 368:1005–11
2. Otto CM, Knuusisto J, Reichenbach DD, Gown AM, O'Brien KD (1994) Characterization of the early lesion of "degenerative" valvular aortic stenosis. Histological and immunohistochemical studies. Circulation 90(2):844–853
3. Leon MB, Smith CR, Mack M, Miller DC, Moses JW et al (2010) Transcatheter aortic-valve implantation for aortic stenosis in patients who cannot undergo surgery. N Engl J Med 363(17): 1597–1607
4. Bonow R, Carabello B, Chatterjee K, de Leon AC, et al (2008) Focused update incorporated into the ACC/AHA 2006 guidelines for the management of patients with valvular heart disease: a report of the American College of Cardiology/American heart association task force on practice guidelines. doi:10.1016/j.jacc.2008.05.008
5. Iung B, Cachier A, Baron G, Messika-Zeitoun D, Delahaye F et al (2005) Decision-making in elderly patients with severe aortic stenosis: why are so many denied surgery? Eur Heart J 26: 2714–2720
6. Chu M, Borger M, Mohr F, Walther T (2010) Transcatheter heart-valve replacement: update. Can Med Assoc J 182(8):791–795
7. Cribier A, Eltchaninoff H, Bash A, Borenstein N, Tron C, Bauer F, Derumeaux G, Anselme F, Laborde F, Leon MB (2002) Percutaneous transcatheter implantation of an aortic valve prosthesis for calcific aortic stenosis: first human case description. Circulation 106:3006–3008
8. Leipsic J, Gurvitch R, LaBounty TM, Min JK, Wood D, Johnson M, Ajlan AM, Wijesinghe N, Webb JG (2011) Multidetector computed tomography in transcatheter aortic valve implantation. J Am Coll Cardiol Imaging doi:10.1016/j.jcmg.2011.01.014
9. Lang P, Seslija P, Chu MW, Bainbridge D, Guiraudon GM, Jones DL, Peters TM (2012) US-fluoroscopy registration for transcatheter aortic valve implantation. IEEE Trans Biomed Eng 59(5):1444–1453
10. Delgado V, Ng A, Shanks M, Van Der Kley F, Schuijf J, Van De Veire N, Kroft L, Roos A, Schalij M, Bax J (2010) Transcatheter aortic valve implantation: role of multimodality cardiac imaging. Expert Rev Cardiovasc Ther 8(1):113–123
11. Greenberg RK, Haulon S, O'Neill S, Lyden S, Ouriel K (2004) Primary endovascular repair of juxtarenal aneurysms with fenestrated endovascular grafting. Eur J Vasc Endovasc Surg 27:484–491
12. Tarek D (2009) An evidence-based approach to minimise contrast-induced neuropathy. N Z Med J 122(1299):39–41
13. Kempfert J, Rastan A, Noettling A, Blumenstein J, Linke A, et al Perioperative dynact for improved imaging during transapical aortic valve implantation. Circulation. doi:10.1055/s-0029-1246838
14. Horvath K, Mazilu D, Guttman M, Zetts A, Hunt T, Li M (2010) Midterm results of transapical aortic valve replacement via real-time magnetic resonance imaging guidance. J Thorac Cardiovasc Surg 139(2):424–430
15. Horvath K, Mazilu D, Kocaturk O, Li M (2011) Transapical aortic valve replacement under real-time magnetic resonance imaging guidance: experimental results with balloon-expandable and self-expanding stents. Eur J Cardio-Thorac Surg 39(6):822–828
16. Wood BJ, Zhang H, Durrani A et al (2005) Navigation with electromagnetic tracking for interventional radiology procedures: a feasibility study. J Vasc Int Radiol 16:493–505
17. Manstad-Hulaas F, Ommedal S, Tangen GA, Aadahl P, Hernes TN (2007) Side-branched AAA stent graft insertion using navigation technology: a phantom study. Eur Surg Res 39(6):364–371
18. Abi-Jaoudeh N, Glossop N, Dake M, Pritchard WF, Chiesa A, Dreher MR, Tang T, Karanian JW, Wood BJ (2010) Electromagnetic navigation for thoracic aortic stent-graft deployment: a pilot study in swine. J Vasc Int Radiol 21:888–895
19. Huang X, Moore J, Guiraudon G, Jones DL, Bainbridge D, Renand J, Peters TM (2009) Dynamic 2D ultrasound and 3D CT image registration of the beating heart. IEEE Trans Med Imaging 28: 1179–1189
20. Huber CH, Nasratulla M, Augstburger M, Von Segesser LK (2004) Ultrasound navigation through the heart for off-pump aortic valved stent implantation: new tool. J Endovasc Ther 11:503–510
21. Lang P, Rajchl M, McLeod AJ, Chu MW, Peters TM (2011) Feature identification for image-guided transcatheter aortic valve implantation. In: Proceedings of SPIE Medical Imaging Conference, vol 8316. pp 83162X–83162X-14
22. Luo Z, Cai JF, Wang S, Zhao Q, Peters T, Gu L (2012) Magnetic navigation for thoracic aortic stent-graft deployment using ultrasound image guidance. IEEE Trans Biomed Eng. doi:10.1109/TBME.2012.2206388
23. Sato Y, Nakamoto M, Tamaki Y et al (1998) Image guidance of breast cancer surgery using 3-D ultrasound images and augmented reality visualization. IEEE Trans Med Imaging 17:681–693
24. Welch JN, Johnson JA, Bax M, Badr R, Shahidi R (2000) A real-time freehand 3D ultrasound system for image-guided surgery. In: Proceedings of the IEEE ultrasonic symposium, San Juan, Puerto Rico, pp 1601–1604
25. Lindseth F, Tangen GA, Langø T et al (2003) Probe calibration for freehand 3-D ultrasound. Ultrasound Med Biol 29:1607–1623
26. Frantz DD, Wiles AD, Leis SE, Kirsch SR (2003) Accuracy assessment protocols for electromagnetic tracking systems. Phys Med Biol 48:2241–2251
27. Wierzbicki M, Drangova M, Guiraudon G, Peters T (2004 Sep) Validation of dynamic heart models obtained using non-linear registration for virtual reality training, planning, and guidance of minimally invasive cardiac surgeries. Med Image Anal 8(3): 387–401

28. Yuan, J, Bae, E, and Tai, X (2010) A study on continuous max-flow and min-cut approaches. In [IEEE conference on computer vision and pattern recognition], IEEE computer society conference on computer vision and, pattern recognition, pp 2217–2224
29. Rajchl M, Yuan J, Ukwatta E, Peters TM (2012) Fast interactive multi-region cardiac segmentation with linearly ordered labels. In: International symposium on biomedical imaging (ISBI), 2012 IEEE International Conference on
30. Cai JF, Luo Z, Gu L et al (2010) The implementation of an integrated computer-assisted system for minimally invasive cardiac surgery. Int J Med Robotics Comput Assist Surg 6:102–112
31. Northern Digital Inc. (2007) Aurora User Guide. Northern Digital: Waterloo, Canada
32. John M, Liao R, Zheng YF, et al. System to Guide Transcatheter Aortic Valve Implantations Based on Interventional C-Arm CT Imaging. Med Image Comput Comput Assist Interv. doi:10.1007/978-3-642-15705-9_46
33. Li N, Beck T, Chen J, Biermann C, Guo L, Sun H, Gao F, Liu C (2011) Assessment of thoracic aortic elasticity: a preliminary study using electrocardiographically gated dual-source CT. Eur Radiol 21:1564–1572